NASA TECHNICAL NOTE

NASA TN D-3911

NASA TN D-3911

LUNAR ORBIT MISSION ANALYSIS FOR THE IMPROVED DELTA LAUNCH VEHICLE AND AIMP-D SPACECRAFT

by

D. L. Mootchnik

Douglas Aircraft Company, Inc.

and

J. Kork

Goddard Space Flight Center

NATIONAL AERONAUTICS AND SPACE ADMINISTRATION • WASHINGTON, D. C. • MAY 1967

NASA TN D-3911

LUNAR ORBIT MISSION ANALYSIS FOR THE IMPROVED DELTA LAUNCH VEHICLE AND AIMP-D SPACECRAFT

By D. L. Mootchnik

Douglas Aircraft Company, Inc.
Santa Monica, Calif.

and

J. Kork

Goddard Space Flight Center
Greenbelt, Md.

NATIONAL AERONAUTICS AND SPACE ADMINISTRATION

For sale by the Clearinghouse for Federal Scientific and Technical Information
Springfield, Virginia 22151 – CFSTI price $3.00

ABSTRACT

A detailed analysis was conducted for the AIMP-D spacecraft mission to determine the launch conditions and trajectory shaping which would maximize the probability of attaining a lunar orbit with a lifetime in excess of six months. This study arose from the relatively large transfer-orbit injection errors which are associated with the spin-stabilized solid propellant injection motor. No midcourse correction is available; the only control parameter is the time of firing of the fixed-impulse lunar orbit injection motor. The large errors resulted in analysis and solutions peculiar to this mission trajectory. It was found that for the applicable vehicle errors, maximum lunar orbit probability was obtained for a 72-hour flight time and a high injection flight path angle. A circular parking orbit could not be used because of the flight path angle requirement and the available launch times were thereby restricted. Analysis of the spacecraft and guidance constraints resulted in the selection of two launch periods, each of several days duration, occurring twice a year.

CONTENTS

LUNAR ORBIT MISSION ANALYSIS FOR THE IMPROVED DELTA LAUNCH VEHICLE AND AIMP-D SPACECRAFT*

by
D. L. Mootchnik
Douglas Aircraft Company, Inc.
and
J. Kork
Goddard Space Flight Center

INTRODUCTION

Certain results of the Improved Delta AIMP-D Spacecraft Lunar Orbit Mission Analysis (Reference 1) are discussed in this paper. The mission involves the placement of a payload consisting of an instrument package and a fourth stage retro motor into a translunar orbit by means of the three-stage Delta boost vehicle. In the vicinity of the moon, the spin-stabilized, fixed-impulse retro motor reduces the approach velocity, thereby causing capture of the spacecraft in a closed lunar orbit.

Because of the high reliability of the Delta vehicle and the limited spacecraft weight capability, a basic management decision was made to minimize vehicle and guidance system hardware modifications. The addition of a midcourse correction system was precluded by this decision. Consequently, the trajectory errors introduced by the boost vehicle, particularly by the spin-stabilized solid propellant third stage, will propagate through the transfer trajectory and cause large, nonlinear dispersions in the moon's vicinity. These potential large dispersions and the availability of only one control parameter, viz., fourth stage ignition time, have led to analysis methods and results unique to this lunar mission.

The primary purpose of the mission analysis was to determine the launch conditions and trajectory shaping which would optimize the probability, for the given spacecraft weight, of obtaining a lunar orbit with a lifetime in excess of six months. Orbit lifetime is the period from lunar orbit insertion to the time when the spacecraft either escapes the moon's vicinity or impacts the lunar surface. Because of the trajectory dispersions and large orbit perturbations caused by the

*This paper is based on work accomplished by the Douglas Aircraft Company, Missile and Space Systems Division, under Contract NAS7-265 (CCN 5) for Goddard Space Flight Center.

earth, a short lunar orbit lifetime is of primary concern in this analysis. A number of additional constraints were imposed on the mission, including the following:

1. The angle between the spacecraft spin axis and the spacecraft sunline is to be between 30 and 150 degrees for the first six months.
2. The spacecraft is to be in sunlight during the last 15 hours of the transfer orbit.
3. The spacecraft is to be visible from the earth at the time of retro firing.
4. The spacecraft shadowing in lunar orbit is to be less than 2.5 hours per orbit revolution.

Analysis showed that the first three constraints result in launch time restrictions, while the shadow time, which depends greatly on retro rocket firing time, trajectory dispersions, and orbit evolution, is not amenable to simple analysis.

FLIGHT PLAN

The basic elements of the flight plan are depicted in Figure 1. In the general description of the flight plan and vehicle given in the paragraphs below, the events and sequence are correct; however, the specific event times are approximate and depend on final vehicle definition and trajectory shaping.

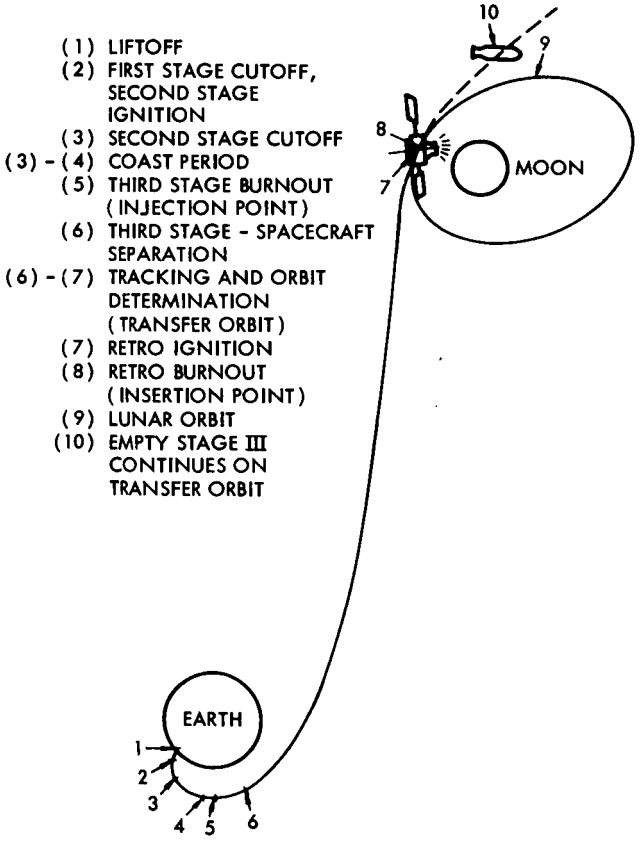

Figure 1—Flight plan of AIMP-D.

A three-stage Improved Delta (Model DSV-3E) will be used as the boost vehicle. The first stage consists of a modified Thor booster with three strap-on TX-33 solid rocket motors; its main propulsion system is a MB3 engine utilizing LOX and RP-1 propellants. The second stage is powered by an AJ10-118 engine. In the first and second stages, the main engines are gimballed for pitch and yaw control, while roll control is maintained by vernier engines and by cold gas nozzles, respectively. The second stage cold gas nozzles also provide full attitude control during the coast period. The third stage is a spin-stabilized solid propellant X-258 motor which is mounted on a spin table mechanism attached to the second stage. A shroud on the second stage encloses the third stage and spacecraft during the ascent in the atmosphere. During first and second stage powered flight and during the second stage coast period, the booster attitude and

sequencing is controlled by a pre-programmed autopilot. A radio guidance system which corrects propulsion and autopilot deviations operates during portions of the first and second stage powered flight.

Upon launch the vehicle travels vertically for four seconds, during which time a roll program causes the vehicle to roll from the pad azimuth to the initial flight azimuth $\left(A_{z_L}\right)$. After four seconds, the programmer stops the roll program and starts the booster pitch program, which consists of four sequential pitch rates varying in magnitude and duration. The pitch program is designed to cause the vehicle to follow approximately a ballistic flight path (i.e., zero angle of attack). The three strap-on solid propellant motors attached to the booster burn out 40 seconds after liftoff and are dropped from the booster at 70 seconds after liftoff. Main engine cutoff (MECO) occurs approximately 150 seconds after liftoff. Upon MECO, the main engine thrust tails off and the vernier engines continue burning for approximately nine seconds.

Four seconds after MECO the second stage separates and ignites; three seconds after ignition the pitch program, consisting of two rates sequentially applied to the stage, is initiated. Second stage engine cutoff (SECO) occurs approximately 550 seconds after liftoff.

After SECO the spent second stage, with the third stage still attached, enters a coast period. During this period, the second stage autopilot programmer causes the second-third stage combination to assume the proper attitude for third stage ignition. This maneuver is necessary because the third stage is spin-stabilized and then flown at constant attitude.

At the proper time during this coast period, an automatic timer ignites the spin table rockets on the second stage which "spins-up" the third stage and then provides a signal to separate and ignite the third stage.

At third stage burnout, the payload is on an elliptic transfer trajectory to the moon. After the vehicle coasts for a short time, the third stage-spacecraft separation mechanism is activated, and a spring imparts a separation velocity of approximately 6 feet per second. The spacecraft then continues on the transfer trajectory, during which various ground tracking systems obtain range, range rate, and other data. These data are used in a real time computer program which predicts and updates the transfer orbit, determining the characteristics of the possible lunar orbits and related data as a function of retro rocket firing time. As the spacecraft approaches the moon, the latest data are used to determine an optimum retro rocket firing time. The firing command is sent either directly or through a time-delay device. If continued tracking or telemetry data indicates that the retro rocket did not fire, a second signal is sent immediately. Barring malfunctions or excessive trajectory deviations, an acceptable orbit will be achieved after the retro rocket burns out.

TRANSFER TRAJECTORY DISPERSIONS

Transfer trajectory deviations result from variations in vehicle propulsion and guidance system. Deviations are introduced by the first, second and third stages; however, the largest

contributor by far is the spin-stabilized solid propellant third stage. While the first and second stages are controlled by an autopilot and guidance system, the third stage is subject to uncorrectable errors in the direction and magnitude of thrust and accounts for over 90 percent of the transfer trajectory deviations. These errors are especially pronounced if the ABL X-258 motor is used as the third stage. The X-258 was considered in the mission analysis; however, it is being replaced by the UTC FW-4 motor for the actual flight. The FW-4 motor has considerably less velocity magnitude error (the primary cause of trajectory deviations). Table 1 shows the approximate three-sigma transfer trajectory injection deviations of the X-258 motor. Figure 2 shows two "three sigma ellipses" of transfer pericynthion location resulting from the injection errors. The region can completely encompass the moon; in fact, for very low energy transfer trajectories, it can extent past the critical Hill's surface (Reference 2) or "sphere-of-influence", thus resulting in a transfer for which a lunar capture is not possible. The size of this region is highly dependent on the energy of the nominal transfer trajectory, increasing in length in the low energy region, which is the region of interest because of retro velocity limitations. These large deviations necessitate determining the conditions which optimize the probability of mission success.

Table 1

Transfer Trajectory Injection: Three Sigma Deviations of the X-258 Third Stage Motor.

Quantity	3σ Deviation
Velocity	174 ft/sec
Elevation Flight Path Angle	1.1 deg.
Azimuth Flight Path Angle	1.1 deg.
Altitude	10.5 n.mi.

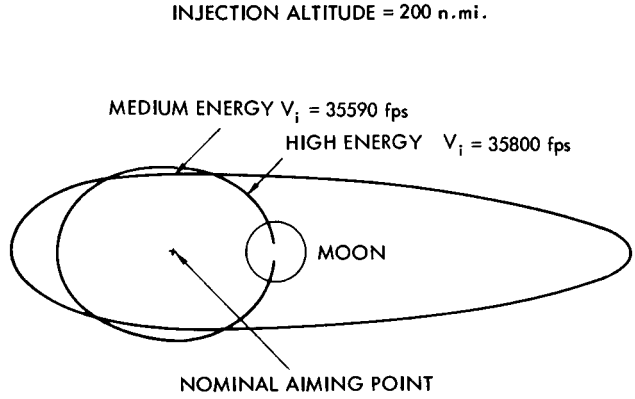

Figure 2–Three-sigma dispersions of the transfer pericynthion.

PROBABILITY STUDIES

The primary purpose of the AIMP-D Lunar Orbit Mission Study was to determine the maximum probability of mission success (P_s) compatible with the vehicle's mode of flight, spacecraft weight, and spacecraft requirements. The basic criterion for determining whether or not a mission is successful is the lifetime of the lunar orbit. Although a lifetime of at least six months is desired, a shorter lifetime would satisfy most mission requirements. The proper choice of a trajectory thus appears to be that which yields the highest curve of lifetime probability history, while favoring a point of the curve corresponding to a six-month lifetime. The basic approach in this analysis was to start with a simplified model in which a wide range of conditions is analyzed, and use the resulting data for a more complicated analysis in the smaller, more interesting region of conditions.

To determine the trajectory which maximizes P_s, it was necessary to combine three studies. These studies were aimed at determining the following:

1. the performance capability of the vehicle,
2. the lunar orbit dispersions about each nominal trajectory,
3. the orbit lifetime resulting from the lunar orbit dispersions.

Since the studies were lengthy and the time for the combined analysis was limited, each study was started at about the same time and accomplished generally independently of the others. Thus, nominal trajectory conditions for the lunar orbit dispersion study were chosen without regard to vehicle capability. This approach was continued until a good understanding of the separate studies was available. Data from the various studies were then combined, for the region of interest, to obtain the final results. This paper is concerned with the second and third of the study phases listed above. Presented below are, first, results of approximate analytic studies on lunar orbit dispersions, and then results of a more sophisticated Monte Carlo analysis of these dispersions. These studies determined the trajectory parameters which affect mission success probability, their relative importance, and an understanding of the effects so that the results could be extrapolated and the conditions optimized.

Probability Study Variables

In setting up the study, one of the major considerations was the choice of a set of parameters to be used as input or independent variables. This set must be sufficiently complete to allow all of the basic effects of the problem to be analyzed, but must also be as small as possible (i.e., no redundancies) in order to reduce the size of the study. Many such sets may be defined: one of them consists of the translunar trajectory injection position, velocity, attitude, time, and the retro velocity, i.e., h_i, ρ_i, μ_i, V_i, γ_i, A_{Z_i}, θ_i, ψ_i, DATE, t_i, and V_R, where the subscript i denotes injection conditions.*

These eleven parameters completely specify a translunar trajectory and retro into a lunar orbit (retro firing time is considered as a dependent variable). However, if this set were used and each parameter perturbed (one at a time) four times, the number of trajectories which must be studied would be 4^{11}. This number is clearly unacceptable and, as will be seen, unnecessary. The following assumptions are made:

1. The boost trajectory from liftoff to third stage burnout, and the vehicle attitude during boost, lie in a plane.
2. The third stage centerline and the third stage burnout velocity vector are parallel.
3. The spacecraft is not rotated in space after separation from the third stage.

*A full list of symbols is given in Appendix A.

Then injection latitude (ρ_i), longitude (μ_i), and azimuth (A_{z_i}) are functions only of launch azimuth A_{z_L} and the powered flight angle θ_{PF}. Furthermore,

$$\theta_i = \gamma_i ,$$

$$\psi_i = A_{z_i} .$$

Since the assumptions depict very closely the characteristics of an actual boost trajectory, the set of eleven parameters can be reduced to eight parameters.

Further reductions can be made by studying the translunar trajectory. A slightly simplified model which neglects the long-period terms in the lunar motion will be set up. Figure 3 depicts the transfer trajectory with respect to the earth-moon plane.

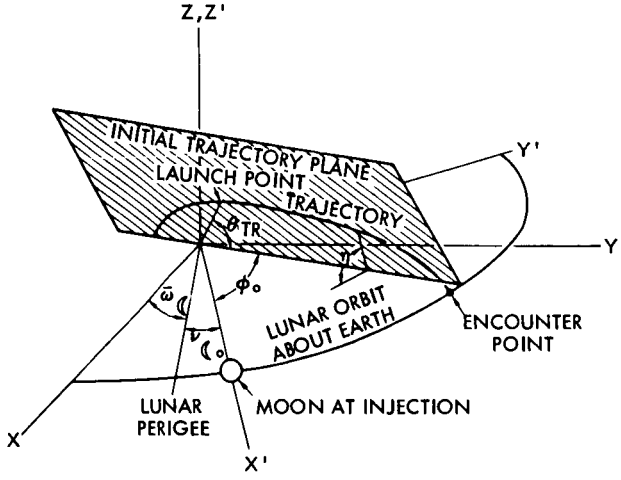

Figure 3—Orientation of the trajectory plane relative to the Earth-Moon plane.

By utilizing the geometry of Figure 3, the injection position vector $[R_i]$ and velocity vector $[\dot{R}_i]$ in the X'Y'Z' coordinate system may be obtained from h_i and V_i by

$$[R_i] = [e_{ij}][h_i + r_e] ,$$

$$[\dot{R}_i] = [f_{ij}][V_i] ,$$

where the transformation elements are

$$e_{ij} = e(\phi_0, \eta, \theta_{TR}) ,$$

$$f_{ij} = f(\phi_0, \eta, \theta_{TR}, \gamma_i) ,$$

and ϕ_0, η, and θ_{TR} are as shown in Figure 3.

The motion of the satellite is a function of $[R_i]$, $[\dot{R}_i]$ and the position history of the moon. If the lunar orbit is assumed circular, then the rotation rate and the earth-moon distance are constant and the position history of the moon after injection may be considered to be independent of injection time and date in the X'Y'Z' coordinate system. Using the above relationships, the trajectory after injection depends on ϕ_0, η, θ_{TR}, γ_i, h_i, V_i, and V_R. Two of these elements, ϕ_0 and θ_{TR}, were not compatible with inputs to the computer programs and were converted by noting that, for trajectories which pass within some distance of the moon, the one-to-one relationships

$$\phi_0 = \phi_0 (r_P, \rho_P) = \phi_0 (b, \rho_b) ,$$

$$\theta_{TR} = \theta_{TR} (r_P, \rho_P) = \theta_{TR} (b, \rho_b) ,$$

can be written if the other elements are kept constant. Further, an analysis of the matched conic solution showed, for a range of injection altitudes on the order of one-tenth the earth radius, that to a very close approximation that the transfer orbit characteristics are similar if orbit energy is fixed. Thus, injection velocity and altitude are related, and if a reference altitude is fixed the above set reduces to $[V_i, \gamma_i, r_P, \rho_P, \eta, \text{and } V_R]$. These six elements then replace the original eleven elements. They were used in the remainder of the studies.

The launch date was deleted from the set of independent parameters which govern the transfer trajectory by assuming the moon to be in a circular orbit. The actual orbit has an eccentricity of about 0.054; thus the earth-moon distance varies by about ±11,400 nautical miles from its mean value. A matched conic sensitivity study revealed that this variation has a second-order effect on the results.

Two-Dimensional Retro Rocket Analysis

A two-dimensional, simplified model was used in an analysis to define, in general terms, the major problems associated with the lunar transfer and capture (via retro rocket) phases of the trajectory. While the data generated in this analysis were not exact, they were sufficiently accurate for accomplishment of the objective of the analysis; i.e., to determine the approximate values of the transfer trajectory parameters which would result in acceptable lunar orbits, thereby narrowing the range of variables to be investigated in the more detailed subsequent analyses.

The matched conic model used in this analysis is two-dimensional, viz., the transfer orbit, retro rocket velocity increment (V_R), and final lunar orbit are defined to be in the plane of the moon about the earth. The moon's motion about the earth is assumed to be described by a circular orbit of radius $(r_{\mathbb{C}})$.

The problem begins at injection into the transfer orbit, which corresponds to the Delta booster third stage burnout. The injection parameters given are radius (r_i) or altitude (h_i), velocity (V_i), and elevation flight path angle (γ_i), measured from a nonrotating geocentric frame (Figure 4). Given these parameters and Keplerian orbit relationships, a vectorial addition can be used to define the velocity vector with respect to the moon. By assuming that the angle between the earth-vehicle line and the earth-moon line is negligible, the following relations can be derived at the SOI (Figure 4):

$$V_{v/\mathbb{C}} = \left[\left(V_{v/\oplus} \cos \gamma'_{v/\oplus}\right)^2 + \left(V_{\mathbb{C}/\oplus} - V_{v/\oplus} \sin \gamma_{v/\oplus}\right)^2\right]^{1/2},$$

$$\gamma'_{v/\mathbb{C}} = \cos^{-1}\left(\frac{V_{v/\oplus}}{V_{v/\mathbb{C}}} \cos \gamma'_{v/\oplus}\right).$$

The point of contact of the trajectory with the SOI, which has a radius of r_s, can be defined by an angle γ_0. Any value of γ_0 can be obtained by varying the launch time while keeping the

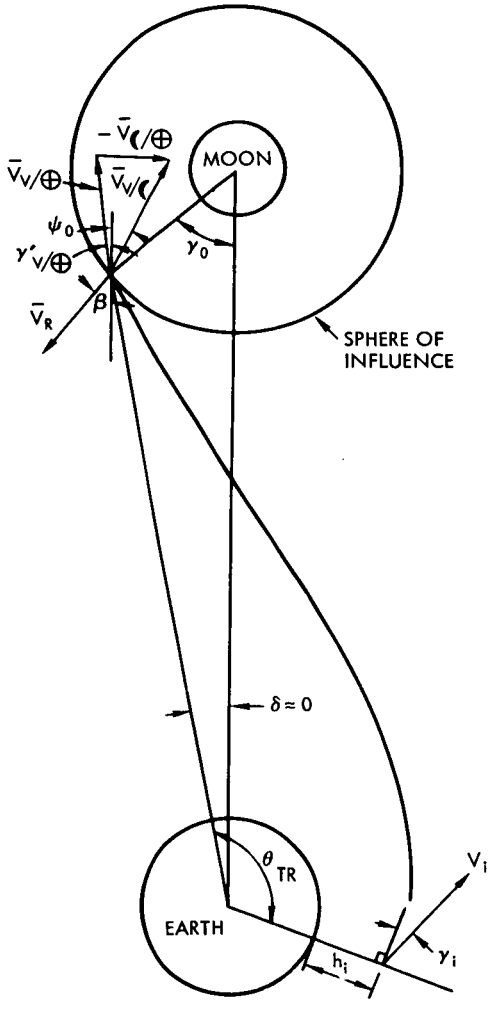

Figure 4—Retro rocket analysis geometry.

transfer trajectory fixed. The impact parameter, b, is given by

$$b = r_s \sin(\gamma'_{v/\mathbb{C}} - \gamma_0) .$$

The above relationships specify the complete lunar transfer orbit.

The one parameter remaining to be defined is the angle β between the retro rocket velocity vector and the earth-moon line. If the retro rocket is assumed to be oriented along the transfer trajectory injection velocity vector, then this angle is

$$\beta = \theta_{TR} + \gamma_i - 90^\circ ,$$

and θ_{TR} is a function of h_i, v_i, and γ_i.

Given the retro rocket velocity magnitude and point (or time) of application, the final lunar orbit can be defined. Thus, all parameters are observed to be functions of the three injection parameters γ_0, V_R and t_R.

The parameters V_i, γ_i, γ_0 and V_R were varied; for each combination the retro velocity was impulsively introduced at various trial times along the transfer trajectory, and the resulting lunar orbit was determined. If one of the trial lunar orbits satisfied the success criterion, then that combination of variables was considered to be acceptable. Results of this portion of the study are presented in Figures 5, 6, and 7 which show the acceptable values of the impact parameter b as a function of transfer injection velocity. For computational purposes an injection altitude of 200 nautical miles is assumed. Positive b indicates a leading edge approach. For the purpose of these figures, a successful orbit is defined as one with a pericynthion altitude greater than 1,000 nautical miles and an apocynthion radius of 25,000 nautical miles or less. The basic quantity to note from these figures is the range $\bar{b}$ of b which yields successful orbits. The amount of trajectory dispersion that can be tolerated is directly related to the width of this range. Errors in b can be related to injection errors; thus these data can be used to establish probability trends.

As shown in Figure 5, for a given V_R and γ_i the limit lines converge with increasing V_i. There is some value of V_i above which no value of $\bar{b}$ exists. No value of $\bar{b}$ exists below the minimum energy case since the transfer trajectory will not reach the sphere of influence.

The effect on the range of b of varying V_R is shown in Figure 5. At the lower velocities, $\bar{b}$ does not change significantly with V_R over a wide range in V_R. The major effect of increasing V_R is to extend the maximum value of V_i at which a successful orbit can be obtained. Above 4,000 fps the effect of V_R is small. A value of 4,000 fps will be used as a basis for the discussion which follows since it approximates the value applicable to the actual spacecraft weights of interest.

Figure 6 shows that at a given V_i the value of $\bar{b}$ increases with increasing γ_i. Since the dispersions in b are not, to the first order, dependent on γ_i (References 1 and 3), an increase in probability can be expected with increasing γ_i. It may be shown that only θ_{TR} and β are significantly affected by γ_i. Since varying θ_{TR} varies the nominal value of b, and this may then be readjusted by changing the initial phase angle, the results indicate that the effect of increasing γ_i is to align V_R more nearly in direct opposition to $V_{V/C}$. Thus the trend of $\bar{b}$ resulting from a change in γ_i is the same as the trend resulting from reorientation of the retro rocket. At V_i equal to 35,500 fps and γ_i equal to 0 degrees, the angle of attack at the SOI (α_{SOI}) is about 36 degrees.

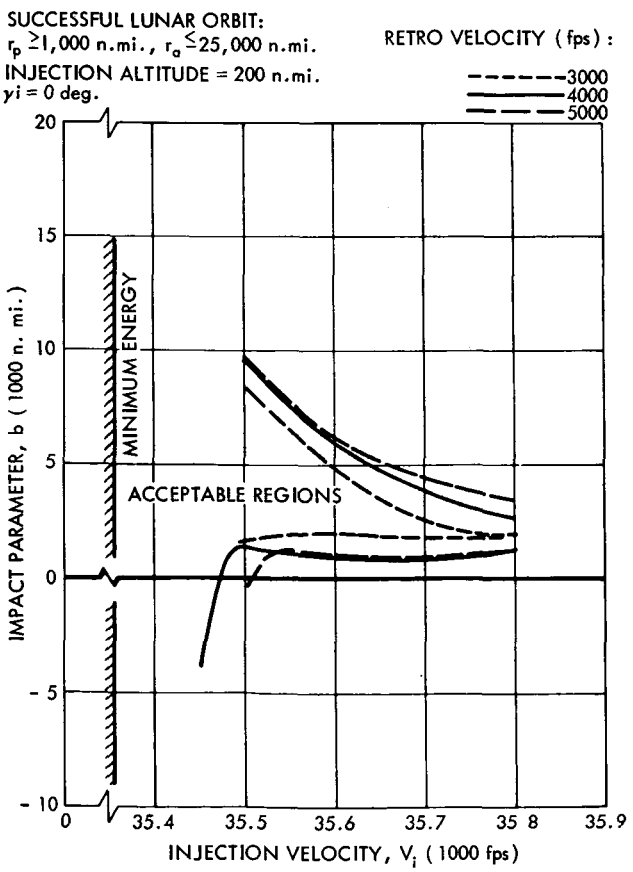

Figure 5—Effect of retro velocity on the allowable transfer trajectory impact parameter for successful lunar orbit insertion.

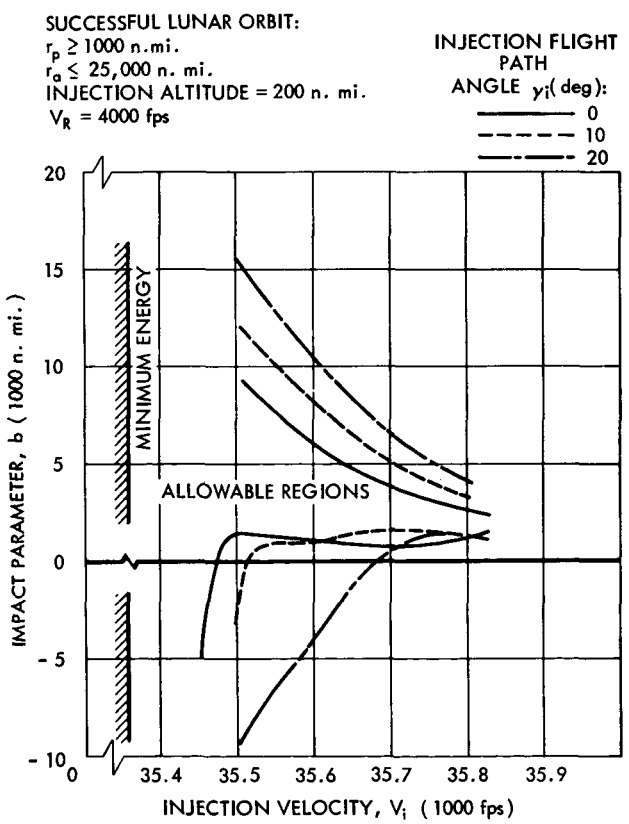

Figure 6—Effect of injection flight path angle on the allowable transfer trajectory impact parameter for successful lunar orbit insertion.

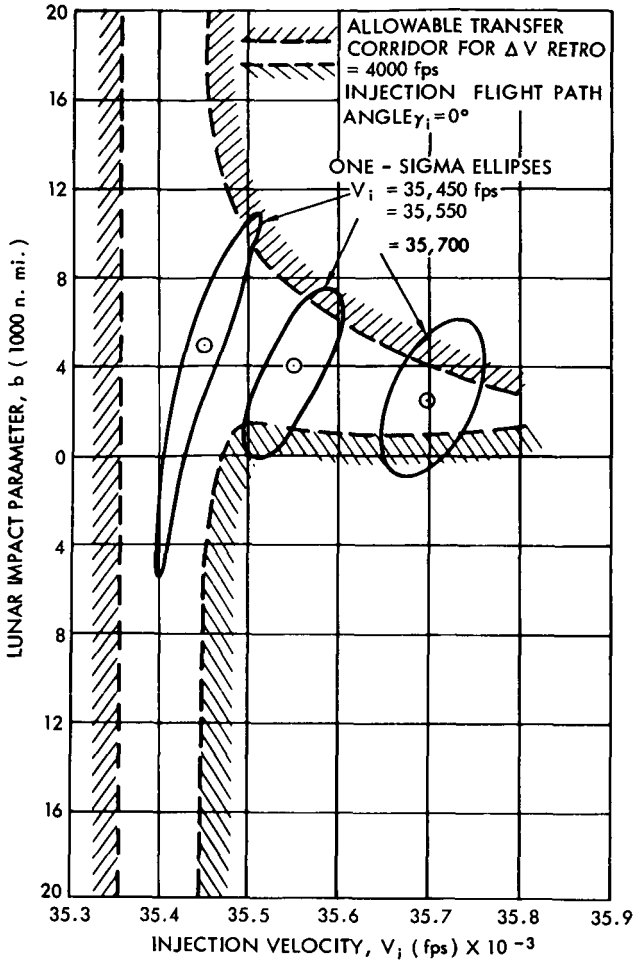

Figure 7—Effect of injection velocity on the probability of successful lunar orbit.

The nominal aiming point to maximize the probability of obtaining a successful orbit should be one which yields a value of b approximately midway in the range of $\bar{b}$. As shown in Figures 5 and 6, this aiming point in general corresponds to a leading edge approach. For high γ_i and low V_i, $\bar{b}$ becomes extremely large and the location of the midpoint is not obvious.

The above data basically define two-dimensional corridors in which transfer to a successful lunar orbit may be achieved. By combining these data with lunar impact sensitivity data (References 1 and 3), an indication of the probabilities of successful lunar orbit may be obtained. The sensitivity data relate transfer orbit injection errors to their effects on the lunar impact parameter. The application of these injection sensitivities to a specific transfer corridor is illustrated in Figure 7.

The transfer corridor selected to illustrate this method is defined by an injection flight path angle of zero degrees and a retro rocket velocity increment of 4,000 fps. Examination of the corridor presented in Figure 7 again shows a generally increasing corridor width for a decreasing injection velocity. From an injection velocity of 35,450 fps to a minimum transfer velocity of 35,350 fps, the corridor widens to 40,000 nautical miles (the value of r_s considered for this study). Thus, one expects a greater allowable injection-impact parameter sensitivity in the lower injection energy regions.

The "elliptic" regions presented in Figure 7 define the impact parameter dispersion for one-sigma variations in vehicle performance at transfer orbit injection corresponding to the velocity and flight path angle errors given in Table 1. The nominal aiming points assumed for the three injection velocities are indicated by point circles. The ellipses may be adjusted vertically by simply changing the launch time (phase angle). An indication of the probability of successful lunar orbit may be obtained by considering the ratio of the dispersion ellipse area within the corridor to the total area of the ellipse. As the injection energy is decreased, the dispersion ellipses are elongated. Thus, the advantage of an increasing corridor width for a decreasing injection velocity is somewhat negated by the increase in dispersion ellipse length. For the specific corridor presented, the one-sigma dispersion ellipses indicate that some velocity in the 35,400 to 35,475 fps

region exists at which the probability of lunar orbit will reach a maximum. Lower nominal V_i are not considered since errors greater than minus one-sigma would extend below the minimum energy velocity.

In summary, the two-dimensional analysis indicated that the optimum injection velocity would be in the low energy region and that the probability of success will be significantly affected by the injection flight path angle. This latter point will be discussed in detail below.

Monte Carlo Analysis

Having limited the variables of concern and having determined the region of interest and an understanding of certain trends, the probability studies were continued using more exact and detailed techniques. This portion of the probability study was accomplished with a three-body trajectory simulation Monte Carlo program. At the outset of the study, a choice was made between using an approximate matched conic solution to the transfer trajectory or a numerically integrated trajectory solution. The former, though approximate, has the advantage of requiring less machine time. The choice was made to use numerical integration for the following reasons:

1. An "exact" solution would in any case have to be programmed to check the approximate answers, and study time was relatively short.
2. While the risk of using an approximate technique in a new application could be taken in a feasibility study, it was felt that this risk could not be afforded at the time of this study phase.

Familiarity with the matched conic technique and the newer asymptotic solutions (Reference 4) obtained during the course of this study would in all probability have resulted in another course of action.

Figure 8 is a block diagram showing the basic flow of the Monte Carlo computer program. The program integrates forward along the trajectory from some initial reference time; for explanatory purposes this time is defined as the second stage burnout time. Nominal initial velocity, position, time, and attitude components are entered. In addition, the standard deviations $\sigma\epsilon_i$ of the statistically independent vehicle parameters ϵ_i which affect the initial conditions are entered, along with the partial derivatives of the initial conditions to variations in these parameters.

To obtain sample initial conditions, n random Gaussian N_i are generated and combined with the above data. After determining the sample initial conditions, the program integrates forward to third stage ignition. At this point three new N_i are generated and used to compute sample third stage thrust and attitude angles. The program then continues integrating through third stage burning and along the subsequent zero thrust transfer trajectory. The distance from the satellite to the moon is checked, and when this distance becomes less than an input value (r_s), the program begins determining the lunar orbit osculating elements which would result if the nominal fourth stage were fired at various points along the trajectory. The program then proceeds to a subroutine which selects the best firing time (discussed below). In this way the program logic parallels the

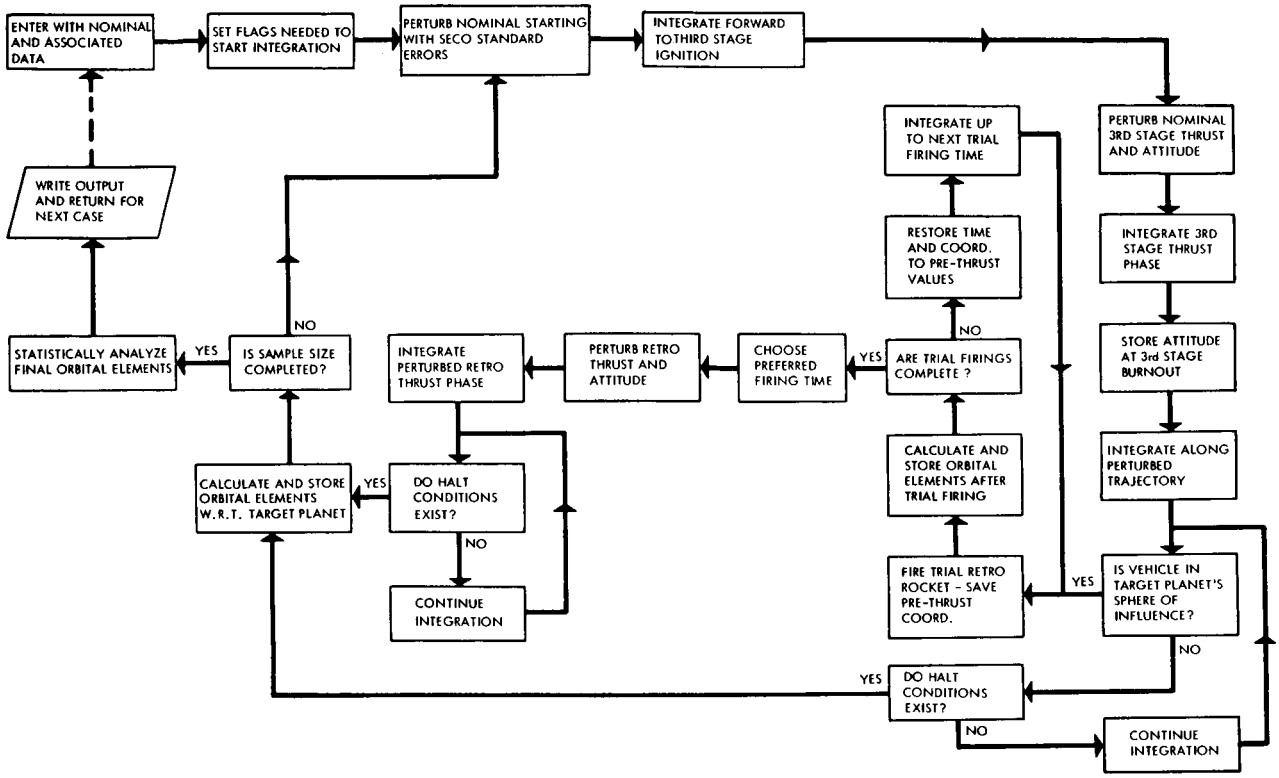

Figure 8—Generalized block diagram of Monte Carlo Interplanetary Trajectory Program.

decisions which would be made during the actual flight. Upon selecting the best firing time, the program generates randomly perturbed fourth stage conditions and computes the resulting sample burnout lunar orbit osculating elements. The program then returns, generates new random numbers for the initial conditions, and repeats the total cycle until the input sample size is reached. The statistical distributions of apocynthion radius (r_a), pericynthion radius (r_p), eccentricity, inclination and the conditional (r_p) distributions for those orbits with $r_a \leq r_{Q_i}$ $(i = 1 \ldots 10)$, where r_{Q_i} are input numbers, are then determined.

At the time of this probability study, the only reliable method available to determine lunar orbit lifetime was the use of several variation-of-parameter programs which numerically integrated the lunar orbit elements. To perform this integration for six-month periods on 5 to 10 trial firing time orbits for each of 100 samples, and then to repeat this procedure for each set of nominal conditions, would require an enormous amount of machine time. Thus, an alternate parameter-to-lifetime relationship was chosen, upon which to determine the firing time for each sample and upon which the probability P_s was calculated. For the firing time determination, two techniques were chosen. The first minimized eccentricity and the second minimized apocynthion radius while restricting the pericynthion to the region above the lunar surface. In both cases the probability of mission success was estimated as

$$P_s = P\left(r_a \leq 25,000 \text{ n.mi.}, r_p \geq 938 \text{ n.mi.}\right) .$$

The optimum probability of obtaining a lunar orbit was investigated by parameterizing the effects of V_i, γ_i, η, r_p, and retro velocity V_R. For computational purposes, the injection conditions are again considered at a reference altitude of 200 nautical miles. The resulting data can be applied to injection at any other altitude by adjusting the velocity to maintain constant transfer orbit energy. December 1965 was originally chosen for the analysis, although the results are applicable for any month. In each lunar month, days exist with equivalent injection conditions. Prior to determining a series of trajectories with varying r_p and ρ_p, impact trajectories were obtained for each of the different injection condition combinations (V_i, γ_i, η). The set of trajectories will be referred to as the impact net.

A set of trajectories, called a miss net, with varying r_p and ρ_p (actually, impact parameter b and its latitude ρ_b were used) was obtained from an impact net trajectory. To determine a trajectory for a given b and ρ_b, A_{Z_L} and t_i were permitted to vary from those values needed for the impact trajectory. Thus the impact trajectory for a given miss net defines the injection conditions V_i, γ_i, η, and a reference flight time t_F, while the individual miss trajectories define r_p and ρ_p or their equivalent b and ρ_b. The launch azimuth and third stage liftoff times were incremented so that the transfer pericynthion locations encompass a grid on the impact parameter (b) surface (that surface which is perpendicular to the incoming approach asymptote).

The orbit probabilities for the trajectories comprising the miss nets were determined by means of the Monte Carlo Interplanetary Trajectory Program. All probabilities investigated in this study were for a sample size of 100. To compensate for the small sample size, several additional and completely independent Monte Carlo studies were performed by utilizing the ITEM trajectory program. In all cases the results compared to within 2 to 4 percent. The fourth stage was trial-fired every hour for 10 hours, the initial firing taking place when the vehicle was approximately 20,000 nautical miles from the moon.

Initially the firing time was chosen on the basis of minimum eccentricity. The result for a typical impact net trajectory is shown in Figure 9. This figure shows contours of constant P_s on the impact parameter plane defined by varying the nominal aiming point as discussed above. As seen, the optimum aiming point occurs for a leading edge or retrograde transfer orbit and for b approximately equal to 4,000 nautical miles and $\rho_b = 45$ degrees. Similar results were obtained for other values of V_i, γ_i, η, and V_R except at very low values of V_i (35,450 fps). For V_i equal to approximately 35,550 fps and above, the optimum b varied from about 3,000 to 4,000; and ρ_b varied from zero for γ_i equal to zero up to 60 degrees for $\gamma_i = 20$ degrees. At $V_i = 35,450$ fps, the optimum location of b was erratic, varying from zero to 10,000 n.mi. For the very low energy transfer, the region of capture and dispersion is so large that the only fact known is that the optimum aiming point is near the moon with either a leading or trailing edge approach. These trends are in good agreement with the results of the two-dimensional analysis discussed earlier.

The effects of varying V_r and η are indicated in Figures 10 and 11. Unlike the results of the approximate study it is seen that V_r has a significant effect on P_s for V_r about 4,000 fps. In

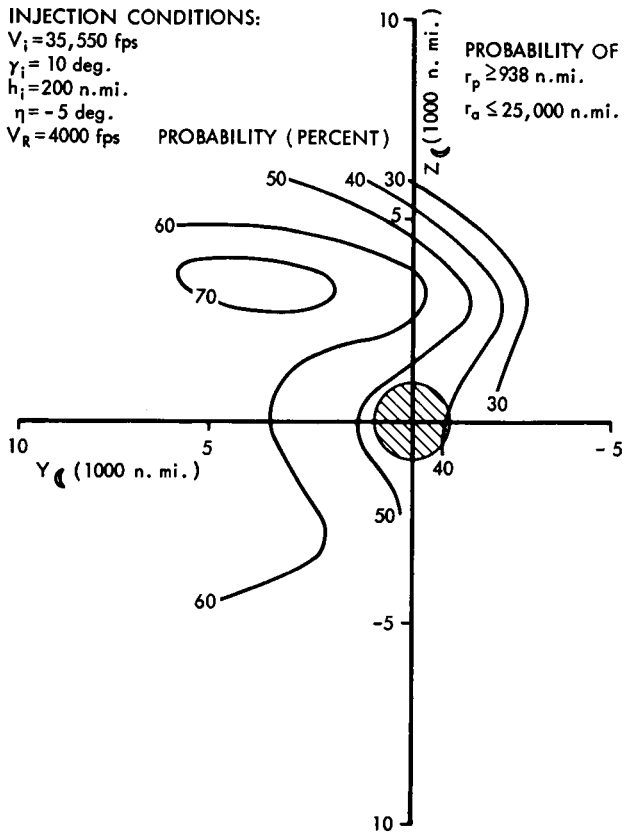

Figure 9—Orbit probability versus impact parameter location.

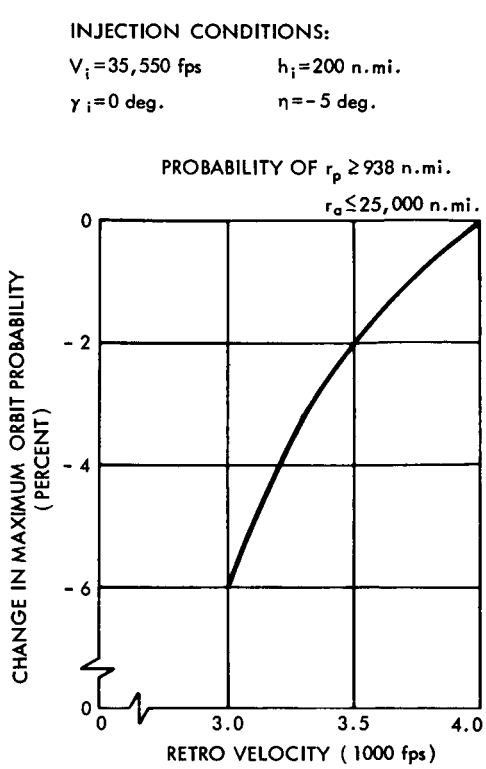

Figure 10—Orbit probability effect of retro velocity.

Figure 11 it is seen that probability decreases with increasing η. This is explained by the fact that the trajectory sensitivity to velocity error increases as η increases. A velocity error has two effects: (1) it changes the true anomaly of the transfer orbit at r_c, and (2) it changes the flight time and thus the moon's position at lunar encounter. For small η's and velocities, these two effects tend to cancel each other vectorially. As η increases, the geometry becomes increasingly three-dimensional and the cancellation effect diminishes.

The data were reanalyzed to determine the effect of the retro rocket firing time determination logic and to better define the optimum. The probability discussed thus far is

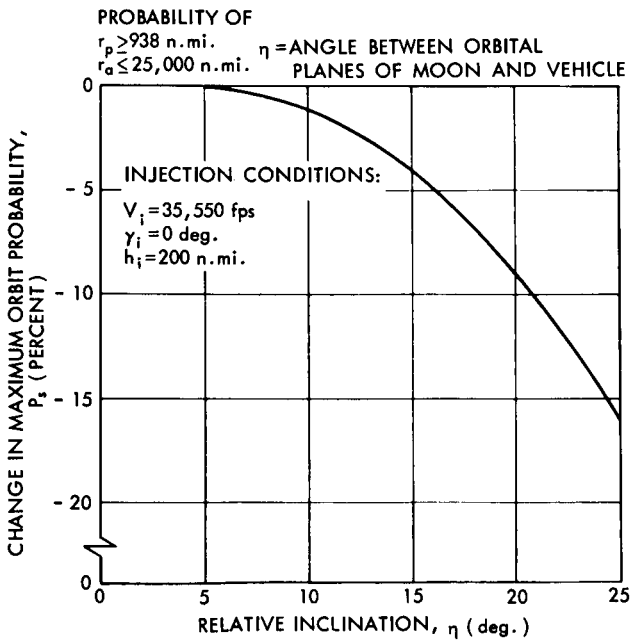

Figure 11—Orbit probability effect of relative inclination on maximum probability.

$$P_s = P\left(r_a \leq 25{,}000 \text{ n.mi.}, r_p \geq 938 \text{ n.mi.}\right) ,$$

while the firing time was determined so as to minimize eccentricity. For this probability, the optimum firing time would be chosen to minimize r_a while maintaining r_p greater than 938 nautical miles. Applying this criterion, typical data are shown in Figures 12 and 13. The new criterion yields higher probabilities; however, the trends with flight path angle and V_i are identical within the accuracy of the results.

For a fixed value of η and V_R, the maximum value of P_s on each miss net was plotted versus injection flight path angle and an energy-related parameter. The parameter chosen was transfer time to impact for the impact trajectory corresponding to each miss net. This parameter had the effect of expanding the scale in the low energy region. The results are shown in Figure 14. The maximum probability is in the range of 65 to 75 hours flight time, which if converted to injection velocity at 200 nautical miles (approximately 35,490 fps to 35,440 fps) is seen to be in close

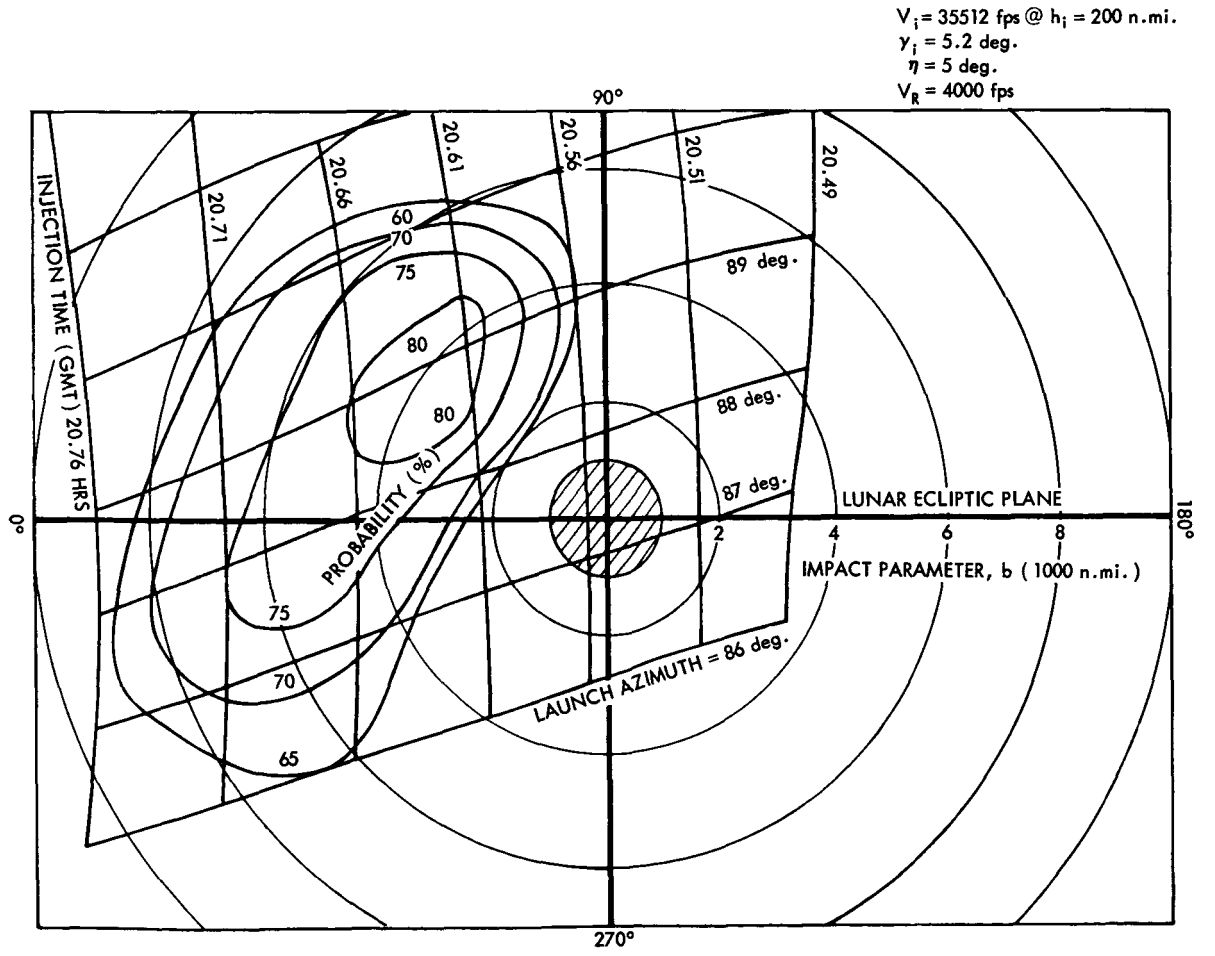

Figure 12—Probability of successful orbit (defined as elliptic orbit with r_a < 25,000 n.mi., r_p > 938 n.mi.) contours on the impact parameter plane.

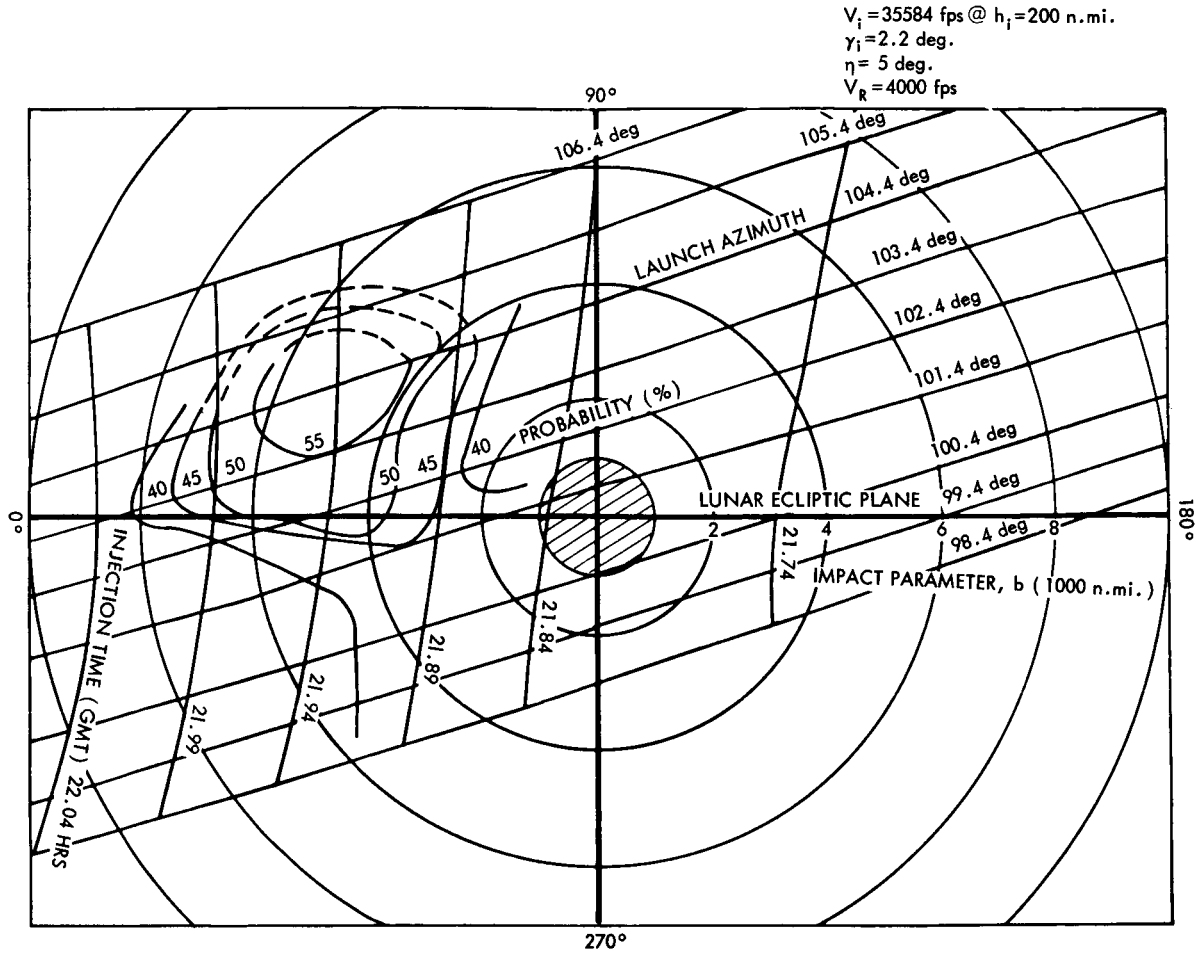

Figure 13—Probability of successful orbit contours on the impact parameter plane.

agreement with the two-dimensional analysis results. Thus the optimum probability of obtaining a lunar orbit occurs for a transfer energy that results in a low enough velocity in the moon's vicinity for the retro rocket to be effective while keeping the transfer dispersions within tolerable limits. In the vicinity of optimum, the curve is rather flat and depends on γ_i, V_R, η, etc.

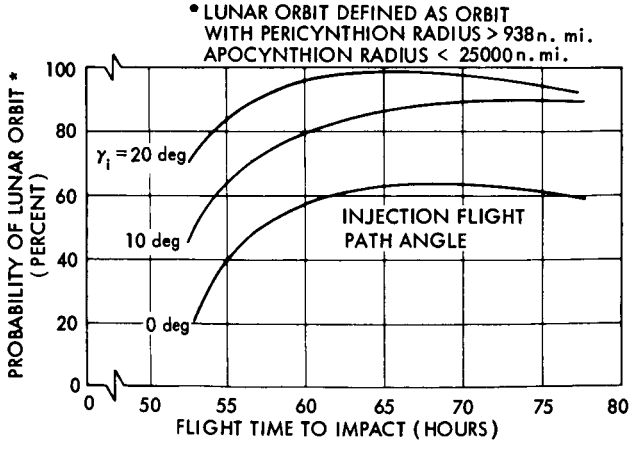

Figure 14—Maximum probability of lunar orbit versus flight time to impact.

It is seen that a P_s of nearly 100 percent can be achieved if an injection flight path angle of 20 degrees or greater is used. Performance optimization studies for the Improved Delta vehicle showed that, for the injection energy of interest, the maximum value of γ_i achievable when the third stage is added along the velocity vector (an assumption inherent in the

results thus far) is between 5 and 6 degrees. Figure 14 shows that this represents an increase of 15 to 20 percent over the zero degree γ_i case. This significant difference immediately rules out the circular parking orbit in favor of an elliptic coast orbit between second stage burnout and third stage ignition.

A study revealed that varying γ_i had only a minor effect on the transfer trajectory sensitivities and approach velocity but that it had a major effect on the relative angle of attack of the retro velocity in the moon's vicinity (Figure 4). At the sphere of influence, since $\gamma_i = \theta_i$,

$$\alpha_{SOI} = \beta - \gamma'_{v/\mathbb{C}} = \theta_{TR} + \gamma_i - 90 - \gamma'_{v/\mathbb{C}} ,$$

$$\frac{\partial \alpha_{SOI}}{\partial \gamma_i} = -2 + 1 - 0.25 \approx -1.25 \text{ deg/deg} .$$

Increasing γ_i rotates V_R toward direct opposition to the approach velocity, $V_{v/\mathbb{C}}$. Monte Carlo runs indicated that a change in α_{SOI} had a significant effect on P_s. For the cases of interest, α_{SOI} was about 36 degrees for γ_i equal to zero.

In order to further improve the value of γ_i or α_{SOI}, the effects of pitching the third stage so that its angle of attack α_3 is non-zero was investigated. For this case α_{SOI} is written as

$$\alpha_{SOI} = \theta_{TR} + \theta_i - 90 - \gamma'_{V/\mathbb{C}} ,$$

and it is noted that

$$\frac{\partial \gamma_i}{\partial \theta_i} = \frac{\Delta V_3}{V_i} \cos \alpha_3 \approx 0.25 \text{ deg/deg} ,$$

and

$$\frac{\partial \alpha_{SOI}}{\partial \theta_i} = \frac{\partial \theta_{TR}}{\partial \gamma_i} \frac{\partial \gamma_i}{\partial \theta_i} + 1 - \frac{\partial \gamma'_{v/\mathbb{C}}}{\partial \gamma_i} \frac{\partial \gamma_i}{\partial \theta_i}$$

$$= +0.44 \text{ deg/deg} .$$

The positive sign indicates that α_{SOI} decreases and probability will increase if θ_i is decreased in this case. Note that for increasing probability the change in γ_i and θ_i is negative for this case, while it is positive for the above case with γ_i varying, with α_3 equal to zero.

When the third stage angle of attack is increased, velocity errors due to attitude errors increase and for large values of α_3 any gain in α_{SOI} would be lost due to the increase in σV_i. However, at moderate values of α_3 this effect can improve probability as follows. The deviation in pericynthion radius due to attitude error is given by

$$\frac{\partial r_p}{\partial \theta_i} = \frac{\partial r_p}{\partial V_i}\frac{\partial V_i}{\partial \theta_i} + \frac{\partial r_p}{\partial \gamma_i}\frac{\partial \gamma_i}{\partial \theta_i} \quad .$$

Using the impulsive approximation, we have

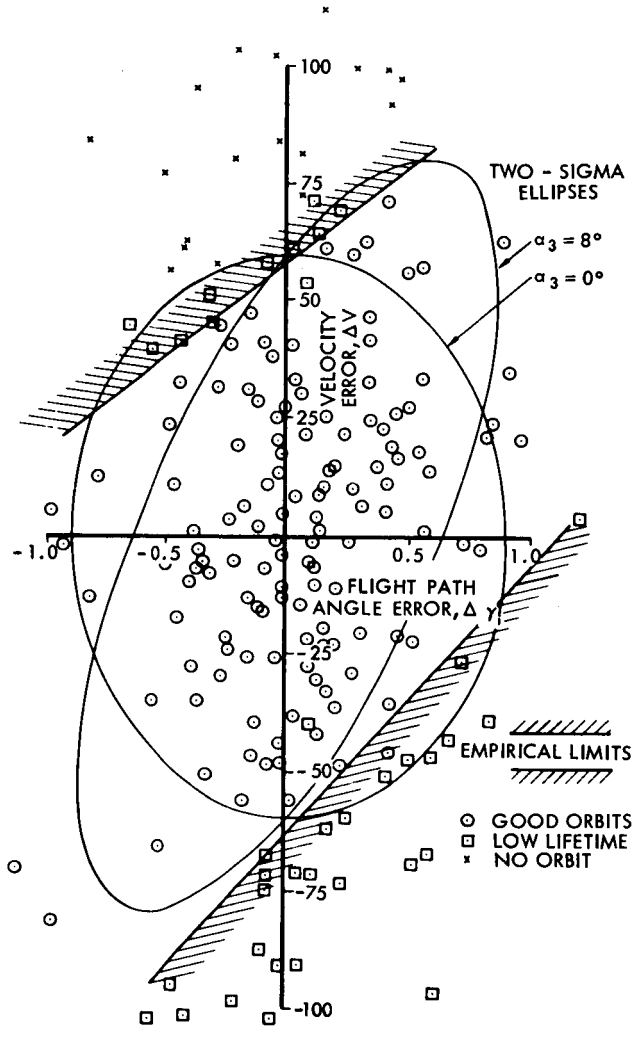

Figure 15—Monte Carlo sample points.

$$V_i^2 = V_{0_3}^2 + \Delta V_3^2 + 2V_{0_3}\,\Delta V_3 \cos\alpha_3 \quad ,$$

$$\gamma_i = \gamma_{0_3} + \tan^{-1}\frac{\Delta V_3 \sin\alpha_3}{V_{0_3} + \Delta V_3 \cos\alpha_3} \quad ,$$

$$\alpha_3 = \theta_i - \gamma_{0_3} \quad ,$$

$$\frac{\partial V_i}{\partial \theta_i} = -\frac{V_{0_3}\,\Delta V_3}{V_i}\sin\alpha_3 \quad ,$$

$$\frac{\partial \gamma_i}{\partial \theta_i} = \frac{\Delta V_3^2 + V_{0_3}\,\Delta V_3 \cos\alpha_3}{V_i^2} \quad .$$

Combining the above equations to eliminate α_3 or θ_i, it can be shown that

$$\frac{\partial r_p}{\partial \theta_i} = 0 \quad ,$$

which would cancel the first order effect of $\sigma\theta_i$ and thus reduce the transfer trajectory dispersion relative to the case with α_3 equal to zero. In addition, increasing α_3 reduces, though only slightly, the effect of σV_3 on σV_i. For this mission the value of α_3 which satisfies the above conditions is about 5 degrees.

Figure 15 shows the results of a typical Monte Carlo run. The samples of ΔV_i and $\Delta\gamma_i$ are shown and the orbit lifetime for each point is indicated. The lifetime information was obtained by a numerical integration program. The region of infinite lifetime is indicated, and approximate two-sigma ellipses are shown for two values of α_3. The trend discussed above is clearly indicated by the percentage of the ellipse area within the good region.

Figure 16 shows the variation of P_s with α_3, for γ_i equal to 1.66 degrees and transfer time equal to about 72 hours. It is seen that approximately a 5 percent increase in P_s is attainable

with an optimum α_3 of 5 degrees. The data clearly indicate the effect of α_3. This figure also shows the effect of σV_i on P_s, which is seen to be quite significant. These data were obtained for a later study, and due to a number of differences not discussed they are not directly comparable to Figure 14.

Recently, an appropriate analytic technique for determining lunar orbit lifetime was developed (Reference 5) and coded. This technique, which requires about 3 seconds of computer time per six-month lunar orbit, is based on the work of Lidov and Williams (References 6 and 7) for the long-period variations, and on a new first order approximation to the bimonthly terms due to earth perturbation. This technique made feasible the use of lunar orbit lifetime calculations to determine the retro firing time and to determine the value of P_s equal to P (lifetime $\geq$ six months) for a wide variety of cases. This technique was used to determine the true value of P_s for the trajectories of Figure 16. The results are shown in Figure 17.

As a last note on probability, the actual launch vehicle will utilize a UTC FW-4 third stage motor which has an estimated σV_3 of about 0.75 the value of the X-258 σV_3. The resulting probabilities are shown in Figures 16 and 17. The actual launch trajectory lies on this curve, with a true P_s value of 89 percent.

LAUNCH WINDOW ANALYSIS

A detailed analysis was performed to determine the trajectory variations and associated performance margin required to obtain launch windows of up to a half hour duration. This study included the determination of the most effective control parameters, correction philosophy, and the trade-offs between loss in spacecraft weight and success probability required

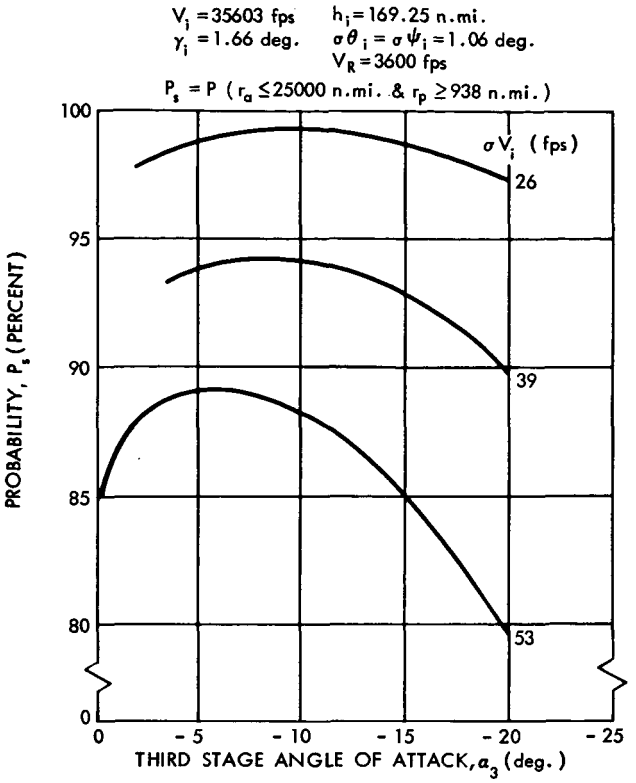

Figure 16—Effect of attitude on orbit probability.

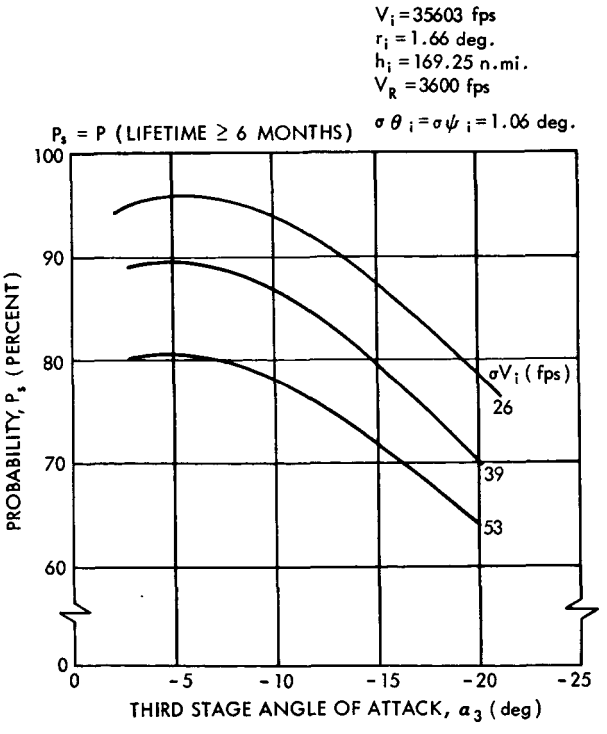

Figure 17—Effect of attitude on orbit lifetime probability.

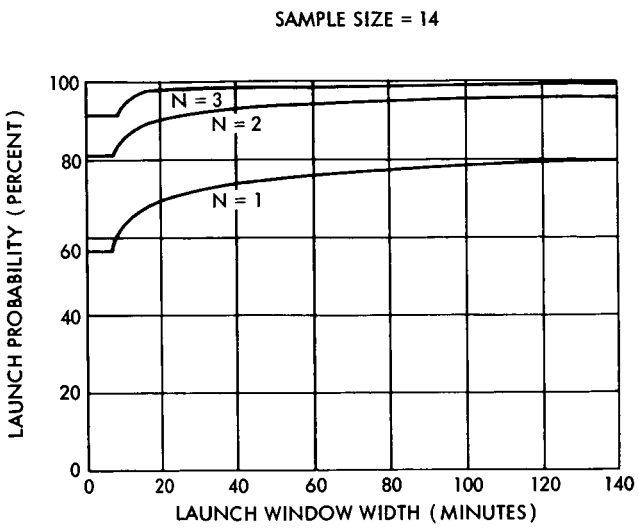

Figure 18—Probability of launch in 'n' consecutive days versus launch window width.

to obtain the necessary performance margin. The results indicated that, at best, a 15-minute launch window would result in a 20 percent loss in P_s or a 12-pound loss in spacecraft weight. Neither loss could be tolerated.

Analysis of past launches revealed that these losses need not occur. The countdown proceedings of 14 Delta launchings were reviewed to determine the history and causes of launch delays, and whether the delay was minutes, one day, or several days. The results are indicated in Figure 18 which shows the launch probability P_e versus launch window for launch periods of one, two and three consecutive days. It is seen that the curves are flat for the first six minutes, and that in order to increase P_e significantly with a launch window, a duration of over 20 minutes is required. The shape of these curves can be explained by noting that if a delay occurs it requires a finite time for correction, and invariably the countdown will be resumed at a point prior to the stopping point. For example, if the count is stopped between T minus one and five minutes, the countdown will be resumed at a pre-specified point, say T minus 15 minutes. Thus, the likelihood of delaying the launch by only one to five minutes was found to be negligble.

It is also seen from Figure 18 that the probability of launching on the first day is 56 percent with an essentially zero launch window. With three consecutive days, the probability is 91 percent, and if two launch periods are available with four days in the first period and three days in the second period, the probability P_e is better than 99 percent. These figures are based on the sample proportion; applying a 90 percent confidence factor, the above number is 95 percent, which is quite satisfactory for mission planning.

Thus, the launch window problem was solved by employing seven launch days divided into two launch periods, with a small window duration of between one and three minutes on each day. The trajectory profile is fixed for each day. The lines of constant injection time in Figure 11 indicate that for these durations the variation in P_s is negligible; since the trajectory is fixed with respect to t_i, no performance margin is needed and thus no spacecraft weight or probability loss occurs.

CONCLUSIONS

In summary, the analysis determined the conditions which would maximize mission success probability, and showed the feasibility of obtaining a lunar orbit without a midcourse correction. It was found that the relative inclination η should be 5 degrees or less, that retro velocity should

be as high as possible, and that a relatively low energy transfer trajectory with a transfer time of about 72 hours should be used. In addition, spacecraft orientation had a significant effect on mission success probability, and in order to optimize this parameter a circular parking orbit could not be used. Finally, it was found that with a sufficient number of launch days, a high probability of launch could be achieved without a significant daily launch window.

Goddard Space Flight Center
National Aeronautics and Space Administration
Greenbelt, Maryland, July 20, 1966
492-05-00-01-51

REFERENCES

1. "Delta IMP-D and E Lunar Orbit Mission Study-Model DSV-3E," Douglas Aircraft Company, Inc., Report No. SM-46345, December 17, 1964.
2. Moulton, F. R., "An Introduction to Celestial Mechanics," New York: MacMillan Company, 2nd ed. rev., 1948.
3. Mickelwait, A. B., and Booten, R. C., Jr., "Analytic and Numerical Studies of Three-Dimensional Trajectories to the Moon," *J. Aerospace Sci.* 27(8):561-573, August 1960.
4. Lagerstrom, P. A., and Kevorkian, J. K., "Earth-to-Moon Trajectories in the Restricted Three-Body Problem," *J. de Mecanique* 2(2):189-218, June 1963.
5. Uphoff, C. W., "An Approximate Method for Predicting Lunar Satellite Lifetimes and its Application to the Delta IMP-D and E Lunar Orbit Mission Study—Model DSV-3E," Douglas Aircraft Company, Inc., Report No. SM-52212, November 1965.
6. Lidov, M. L., "Evolution of the Orbits of Artificial Satellites as Affected by Gravitational Perturbation from External Bodies," *AIAA J. Russian Suppl.* 1(8):1985-2002, August 1963.
7. Williams, R. R., and Lorell, J., "The Theory of Long-Term Behavior of Artificial Satellite Orbits Due to Third-Body Perturbations," Jet Propulsion Laboratory, NASA CR-70738; JPL TR-32-916; N66-18309, February 15, 1966.

Appendix A

Symbol List

A_z	Azimuth, angle between the projections of true north and the velocity vector on the local horizontal plane
b	Impact parameter, closest approach distance to moon assuming a massless moon
h	Altitude above earth's surface
N_i	Random numbers
n	Number of vehicle errors which will perturb SECO conditions
r	Radius
r_e	Earth's radius
$r_{\mathbb{C}}$	Average radius of the moon's orbit above the earth
r_s	Sphere of influence radius, radius from the center of the moon defining the point at which the reference coordinate system is changed and lunar computations commence
$[R_i]$	Injection position vector in earth-moon plane coordinate system
t	Time
t_f	Flight time, time from injection to impact on the associated impact net trajectory
V	Velocity
V_R	Retro impulsive velocity
ΔV_3	Third stage impulsive velocity
α	Angle of attack
β	Angle between $\vec{V}_R$ and earth-moon line
γ	Elevation flight path angle measured from local horizontal
γ'	Elevation flight path angle measured from local vertical
γ_0	Approach phase angle at sphere of influence
ϵ_i	Vehicle error which may affect SECO conditions
$\sigma\epsilon_i$	Standard deviation of ϵ_i
η	Relative inclination, angle between the initial transfer trajectory plane and the earth-moon plane
θ	Orientation angle, angle between vehicle centerline and the local horizontal

θ_{PF} Powered flight angle, angle between the radius vectors from the center of the earth at launch and at injection measured in a non-rotating frame

θ_{TR} Transfer angle, angle between the radius vectors from the center of the earth at injection and at lunar encounter measured in a non-rotating frame

μ Longitude

ν_0 True anomaly of moon at time of injection

ρ Latitude

ρ_b Latitude of closest approach radius vector assuming a massless moon, measured from ecliptic plane

ϕ_0 Phase angle

ψ Orientation angle, angle between the projections of true north and the vehicle centerline on the local horizontal

$\tilde{\omega}_{\mathbb{C}}$ Argument of perigee of the lunar orbit measured from the ascending node of the lunar orbit on the equatorial plane

Subscripts

a Referring to apocynthion

i Referring to injection conditions

L Referring to launch conditions

p Referring to perigee or pericynthion

SOI Referring to sphere of influence conditions

$v/\oplus$ Vehicle with respect to earth

$v/\mathbb{C}$ Vehicle with respect to moon

$\mathbb{C}/\oplus$ Moon with respect to earth

3 Third stage initial conditions

NASA-Langley, 1967 —— 30

10-5-67

"The aeronautical and space activities of the United States shall be conducted so as to contribute . . . to the expansion of human knowledge of phenomena in the atmosphere and space. The Administration shall provide for the widest practicable and appropriate dissemination of information concerning its activities and the results thereof."

—NATIONAL AERONAUTICS AND SPACE ACT OF 1958

NASA SCIENTIFIC AND TECHNICAL PUBLICATIONS

TECHNICAL REPORTS: Scientific and technical information considered important, complete, and a lasting contribution to existing knowledge.

TECHNICAL NOTES: Information less broad in scope but nevertheless of importance as a contribution to existing knowledge.

TECHNICAL MEMORANDUMS: Information receiving limited distribution because of preliminary data, security classification, or other reasons.

CONTRACTOR REPORTS: Scientific and technical information generated under a NASA contract or grant and considered an important contribution to existing knowledge.

TECHNICAL TRANSLATIONS: Information published in a foreign language considered to merit NASA distribution in English.

SPECIAL PUBLICATIONS: Information derived from or of value to NASA activities. Publications include conference proceedings, monographs, data compilations, handbooks, sourcebooks, and special bibliographies.

TECHNOLOGY UTILIZATION PUBLICATIONS: Information on technology used by NASA that may be of particular interest in commercial and other non-aerospace applications. Publications include Tech Briefs, Technology Utilization Reports and Notes, and Technology Surveys.

Details on the availability of these publications may be obtained from:

SCIENTIFIC AND TECHNICAL INFORMATION DIVISION

NATIONAL AERONAUTICS AND SPACE ADMINISTRATION

Washington, D.C. 20546